

High-efficiency generation of Bessel beams with transmissive metasurfaces

Cite as: Appl. Phys. Lett. **112**, 191901 (2018); <https://doi.org/10.1063/1.5023553>

Submitted: 25 January 2018 . Accepted: 20 April 2018 . Published Online: 07 May 2018

Zhuo Wang, Shaohua Dong, Weijie Luo, Min Jia, Zhongzhu Liang, Qiong He, Shulin Sun , and Lei Zhou



View Online



Export Citation



CrossMark

ARTICLES YOU MAY BE INTERESTED IN

Generating millimeter-wave Bessel beam with orbital angular momentum using reflective-type metasurface inherently integrated with source

Applied Physics Letters **112**, 141901 (2018); <https://doi.org/10.1063/1.5023327>

Generation of radio vortex beams with designable polarization using anisotropic frequency selective surface

Applied Physics Letters **112**, 203501 (2018); <https://doi.org/10.1063/1.5029507>

Design of digital coding metasurfaces with independent controls of phase and amplitude responses

Applied Physics Letters **113**, 063502 (2018); <https://doi.org/10.1063/1.5043520>



**THE WORLD'S RESOURCE FOR
VARIABLE TEMPERATURE
SOLID STATE CHARACTERIZATION**



WWW.MMR-TECH.COM

OPTICAL STUDIES SYSTEMS

SEEBECK STUDIES SYSTEMS

MICROPROBE STATIONS

HALL EFFECT STUDY SYSTEMS AND MAGNETS

High-efficiency generation of Bessel beams with transmissive metasurfaces

Zhuo Wang,^{1,a)} Shaohua Dong,^{2,a)} Weijie Luo,¹ Min Jia,¹ Zhongzhu Liang,³ Qiong He,^{1,4} Shulin Sun,^{2,3,b)} and Lei Zhou^{1,4,b)}

¹State Key Laboratory of Surface Physics and Key Laboratory of Micro and Nano Photonic Structures (Ministry of Education), Fudan University, Shanghai 200433, China

²Shanghai Engineering Research Center of Ultra-Precision Optical Manufacturing, Green Photonics and Department of Optical Science and Engineering, Fudan University, Shanghai 200433, China

³State Key Laboratory of Applied Optics, Changchun Institute of Optics, Fine Mechanics and Physics, Chinese Academy of Sciences, Changchun 130033, China

⁴Collaborative Innovation Center of Advanced Microstructures, Nanjing 210093, China

(Received 25 January 2018; accepted 20 April 2018; published online 7 May 2018)

Circularly polarized Bessel beams (BBs) are important in biomolecule-sensing-related applications, but the available generators are too bulky in size and/or exhibit low efficiencies. Here, we design and fabricate ultra-thin ($\sim\lambda/6$) transmissive Pancharatnam-Berry metasurfaces and perform near-field scanning measurements to show that they can generate circularly polarized BBs within a frequency window of 10.7–12.3 GHz. We experimentally demonstrate that the generated BBs exhibit a self-healing effect, illustrating their non-diffraction characteristics. Finally, we employ far-field measurements to demonstrate that the working efficiency of our devices can reach 91%, while the simulated efficiency reaches 92%. All experimental results are in perfect agreement with full-wave simulations.

Published by AIP Publishing. <https://doi.org/10.1063/1.5023553>

Bessel beams (BBs), a special type of non-diffraction beam exhibiting unique self-healing properties, have attracted intensive interest in photonic research, owing to their potential applications in particle trapping and manipulation, near-field probing, photolithography, and so on.^{1–4} Circularly polarized (CP) BBs are particularly useful in sensing and manipulating biomolecules, which typically possess chiral structures.^{5,6} Conventional devices to generate BBs (such as annular slits,⁷ axicons,⁸ and binary holograms⁹) are too bulky in size and/or too inefficient [Fig. 1(a)], being unfavorable for integration into optical applications.

Recently, metasurfaces—planar metamaterials composed of subwavelength meta-atoms with tailored optical responses—have been widely used to reshape the wavefronts of impinging electromagnetic (EM) waves. By designing metasurfaces with appropriate transmission/reflection phase profiles, many fascinating wave-manipulation effects have been realized, such as anomalous refraction/reflection,^{10–12} surface-plasmon excitations,¹³ meta-holograms,^{14,15} and flat-lens imaging.^{16–20} In particular, microwave BB generators have been constructed based on transmissive metasurfaces (i.e., Huygens' surfaces).²¹ However, such devices can only generate linearly polarized BBs, and the involved meta-atoms are *non-flat* three-dimensional (3D) structures, which must be designed on a site-to-site basis. Meanwhile, Pancharatnam-Berry (PB) metasurfaces exhibit many advantages in controlling CP beams since the generated phase distributions on such metasurfaces are independent of frequency, and their design and fabrication are relatively simple as only one meta-atom needs to be designed.^{22–24} Indeed, many interesting effects have been realized with PB metasurfaces, such as the photonic spin-Hall effect,^{25–27} BB

generation,^{21,28} and meta-holograms.^{29–31} However, PB devices (especially in transmission geometry) do not necessarily exhibit high working efficiencies since normal-mode scatterings can also be generated, which possess a spin identical to that of the incident beam [Fig. 1(b)]. The presence of normal modes not only degrades the device's working efficiency but, more importantly, also interferes with the generated BBs to eventually impair the device's functionality. Although high-efficiency BB generators have been proposed based on dielectric metasurfaces at optical frequencies,²³ the thicknesses of such devices are comparable to their wavelength, which can be an issue for low-frequency applications, not to mention the fabrication complexities for such high-aspect-ratio meta-structures.

In this letter, we design and fabricate a microwave BB generator based on a carefully designed transmissive metasurface following a criterion established in our recent work³² and experimentally demonstrate that it can generate BBs with very high efficiency (91%), not suffering from interference by normal modes within a broad frequency band (10.7–12.3 GHz). The fabricated device is ultrathin ($\sim\lambda/6$), flat, and easy to fabricate, and the design principle can be straightforwardly extended to the high-frequency regime. Finally, we experimentally demonstrate that the generated BBs exhibit a self-healing effect after being scattered by a small metallic object.

We start by presenting the guiding criterion to design a 100%-efficiency transmissive PB meta-atom to construct our BB generator. Let r_{xx} , r_{yy} , t_{xx} , and t_{yy} denote the reflection and transmission coefficients of a meta-atom (periodically repeated to form a slab) illuminated by EM waves with different polarizations. Using such a meta-atom as a building block to construct a PB metasurface with a desired phase distribution, our theoretical analyses³² indicate that the device can generate four beams, i.e., normal and anomalous beams

^{a)}Z. Wang and S. Dong contributed equally to this work.

^{b)}Authors to whom correspondence should be addressed: sls@fudan.edu.cn and phzhou@fudan.edu.cn.

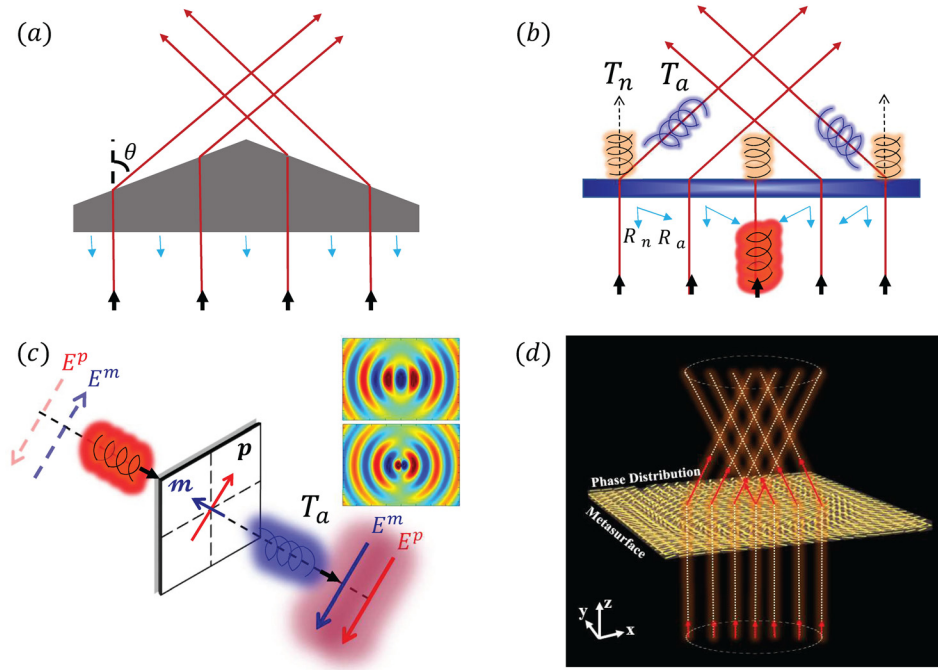


FIG. 1. (a) Working principle of a conventional axicon lens. (b) Drawbacks of a meta-axicon made with a PB metasurface: multi-mode generations and low efficiency. (c) Design principle of a 100%-efficiency transmissive PB meta-atom exhibiting both electric and magnetic responses. (d) A meta-axicon made with a 100%-efficiency PB meta-atom can generate ideal BBs with high efficiencies, without suffering interference from normal-mode waves.

on the transmission and reflection sides of the device. The power efficiencies of these four beams, denoted T_n , T_a , R_n , and R_a correspondingly, are related to Jones' matrix elements via

$$\begin{aligned} T_a &= |(t_{xx} - t_{yy})|^2/4, & R_a &= |(r_{xx} - r_{yy})|^2/4, \\ T_n &= |(t_{xx} + t_{yy})|^2/4, & R_n &= |(r_{xx} + r_{yy})|^2/4. \end{aligned} \quad (1)$$

Only the anomalous-transmission beam is desired, while the others not only drain energy but also interfere with the desired beam's ability to exhibit the needed wave-manipulation functionality [Fig. 1(b)]. To maximize the working efficiency of our device, we need to suppress those undesired modes (i.e., $R_a = R_n = T_n = 0$), leading to the criterion

$$|r_{xx}| = |r_{yy}| = 0, \quad |t_{xx}| = |t_{yy}| = 1, \quad \arg(t_{xx}) - \arg(t_{yy}) = \pi \quad (2)$$

to design our meta-atom. Equation (2) implies that the desired meta-atom should not only be reflectionless for impinging waves with arbitrary polarizations but, more importantly, also work as an ideal half wave-plate in the transmission mode.

We now design a meta-atom according to Eq. (2). Obviously, a single-layer meta-atom exhibiting only an electric-dipole response does not work since the excited dipole can radiate to both sides of the meta-atom, and thus, the reflection can never be suppressed. It is thus crucial for the meta-atom to have both electric and magnetic responses,³² so that the interference between radiations from the two different types of dipoles can suppress the reflection, leading to perfect transmission [Fig. 1(c)]. However, adding vertical split-ring resonators into the meta-atom design²¹ makes the meta-atom structure non-flat and difficult to fabricate. Here, we choose an alternative approach to add magnetic resonances into our meta-atom design. Inspired by our previous works,³² we choose an ABA structure to design our meta-atom [Fig. 2(a)], in which the magnetic resonances are introduced through the

mutual couplings between adjacent layers. Specifically, layer A in our meta-atom is just a metallic bar (width: 0.9 mm and length: 5.2 mm), while layer B is a metallic plate drilled with a circular air-hole (diameter: 5.6 mm) and loaded with the same type of metallic bar as in layer A. Two 2-mm-thick dielectric spacers ($\epsilon_r = 4.3 + 0.01 * i$) are adopted to separate the two adjacent layers. It has been shown in Ref. 32 that such an ABA structure can support multiple solutions of perfect EM-wave transparency when its effective EM responses satisfy certain conditions. Therefore, we can tune the geometrical parameters of the ABA structure to make it perfectly transparent for the two polarizations yet with such transparencies governed by different mechanisms so that the associated transmission phases can be dramatically different. The final design is obtained using full-wave simulations (see the caption of Fig. 2 for the meta-atom's geometrical parameters), based on the above arguments. As shown in Figs. 2(c) and 2(d), FDTD-simulated transmission spectra of the designed meta-atom (periodically replicated to form a slab) do exhibit a common transparency window around 11.8 GHz for the two polarizations, yet the transmission-phase difference between the polarizations remains about 180° within that frequency window (10.7–12.3 GHz). We next compute the efficiencies of four beams based on these transmission and reflection spectra. The results in Figs. 2(e) and 2(f) indicate that indeed only T_a survives, while T_n, R_n, R_a are significantly suppressed within the working band. The maximum working efficiency T_a of this meta-atom reaches 91% at 11.8 GHz, which can be further increased if the dielectric loss can be made even smaller. We fabricate a realistic sample [illustrated in Fig. 2(d)] according to our design and then perform microwave experiments to characterize its Jones' matrix properties. The measured results are in perfect agreement with FDTD simulations (Fig. 2).

We now use the designed meta-atom as a building block to construct our BB generator. A zero-order BB is described by $E_{BB}(\vec{r}, t) = e^{ik_z z} J_0(k_{\parallel} \rho) e^{-i\omega t}$, which can be alternatively

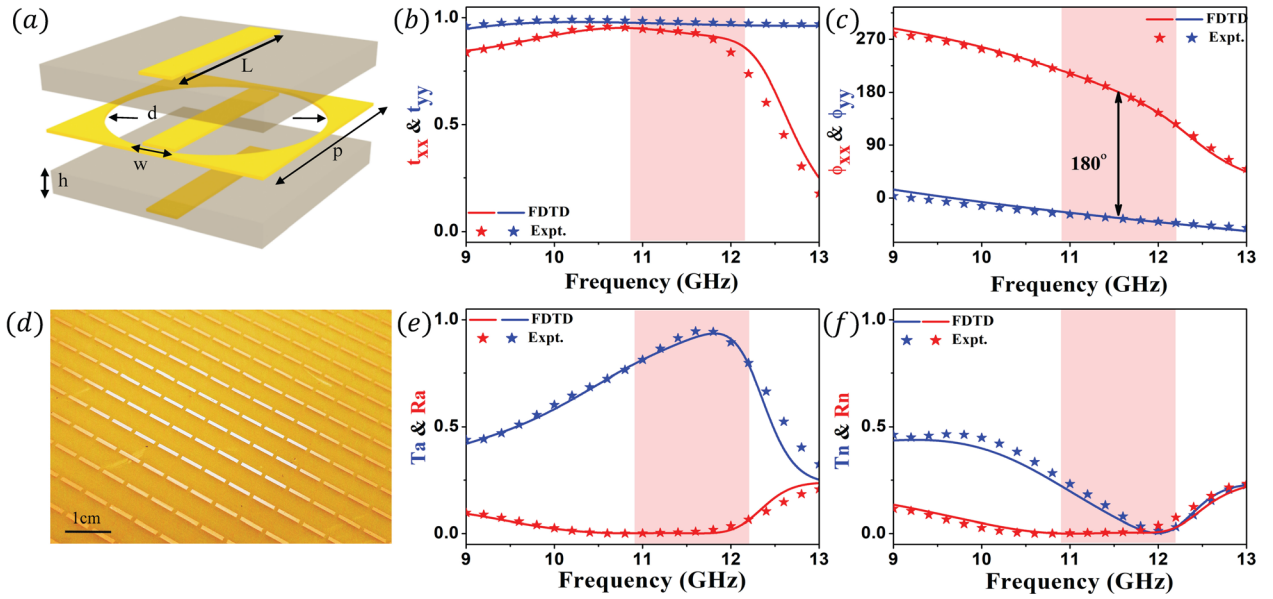


FIG. 2. (a) Geometry of the proposed high-efficiency PB meta-atom, which has an ABA structure with layer A being a metallic bar and layer B being a holey metallic film loaded with a metallic bar. Two 2 mm-thick dielectric spacers ($\epsilon_r = 4.3 - 0.01 * i$) are used to separate adjacent metallic layers. (d) Photograph of part of the fabricated sample consisting of a periodic array of the designed meta-atoms with $p = 6$ mm, $h = 2$ mm, $w = 0.9$ mm, $L = 5.2$ mm, and $d = 5.6$ mm. (b) and (c) Measured and simulated transmission amplitude and phase spectra for the sample shown in (d) for different polarizations. (e) and (f) Spectra of T_a, R_a (e) and T_n, R_n (f) for the PB metasurface depicted in (d) calculated according to Eq. (2).

written as $e^{ik_z z} \times \int_0^{2\pi} e^{ik_{||}(x \cos \varphi + y \sin \varphi)} \frac{d\varphi}{2\pi} \times e^{-i\omega t}$, where $k_{||}^2 + k_z^2 = k_0^2$, with k_0 being the free-space wave-vector, $x^2 + y^2 = \rho^2$, and φ denotes the orientation angle of $\vec{k}_{||}$. This implies that the BB can be formed by a series of plane waves with different wave-vectors $\vec{k} = (k_{||} \cos \varphi, k_{||} \sin \varphi, k_z)$. The conventional approach to generate BBs uses an axicon to symmetrically refract an incident plane wave to an angle $\theta = \sin^{-1}(k_{||}/k_0)$ toward the optical axis of the device [Fig. 1(a)]. Here, we use a PB metasurface exhibiting the transmission-phase distribution

$$\phi(x, y) = k_{||} \sqrt{x^2 + y^2} \quad (3)$$

to replace the axicon. To design the metasurface, we need to arrange the PB meta-atoms in a two-dimensional (2D) plane, with the meta-atom located at point (x, y) exhibiting an orientation angle $\alpha = \phi(x, y)/2$ [Fig. 3(f)]. According to Refs. 27 and 30 when illuminating such an α -orientated meta-atom with left CP light, the wave passing through it will be right CP light possessing an extra phase factor $e^{i2\alpha}$. Figure 3(f) depicts part of the sample fabricated according to the above design.

We next experimentally demonstrate the functionality of our fabricated device. Illuminating the sample normally with left CP waves at different frequencies, we adopt a 1.5 cm-long

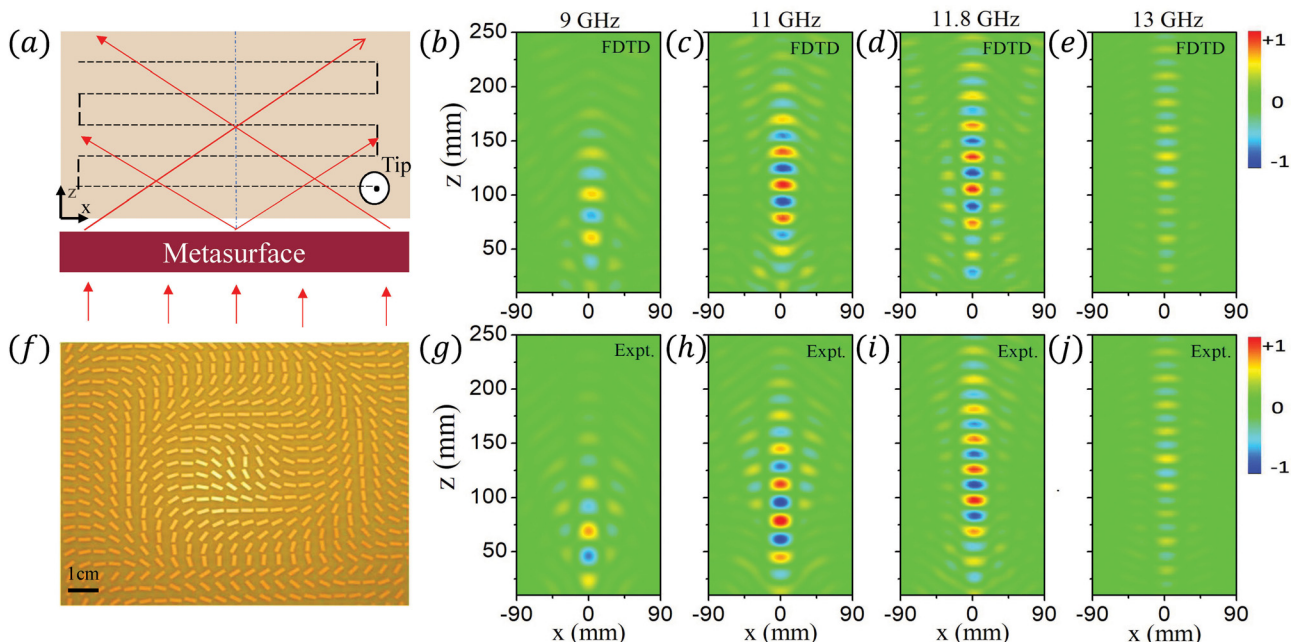


FIG. 3. (a) Schematic of the near-field scanning experiment. (f) Photograph of the fabricated BB generator. E_y field distributions of the generated BBs on the xz -plane at the transmission side of the BB generator, obtained by FDTD simulations (b)–(e) and experimental measurements (g)–(j) at different frequencies.

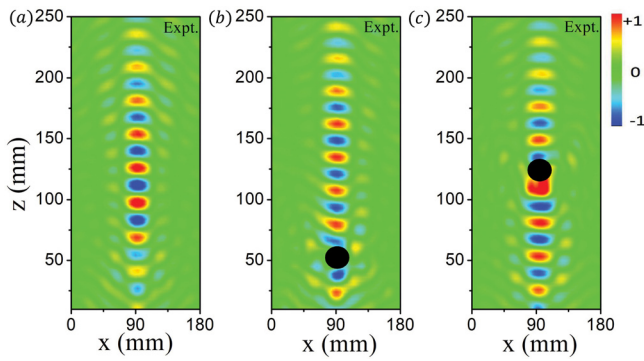


FIG. 4. Experimental verification of the self-healing effect of the generated BB. Measured E_y distributions of the generated BB scattered by a metallic sphere (diameter $D = 15$ mm) placed at (b) 55 mm and (c) 125 mm away from the metasurface, compared with (a) that measured in the absence of the metallic sphere. The frequency is fixed at 11.8 GHz.

monopole antenna to map the distributions of the E field at the transmission side, including both amplitude and phase information. Figures 3(g)–3(j) depict the measured E_y field distributions on the x - z plane (with $y = 0$) at different frequencies. At 11 GHz and 11.8 GHz within the working band, the measured field patterns exhibit very clear non-diffraction features. We note that the “length” of this non-diffraction range increases as the frequency changes from 11 GHz to 11.8 GHz, which is understandable since our device has a finite lateral size, and this finite-size effect is weakened as the frequency increases. Meanwhile, for frequencies outside of the working band (e.g., 9 GHz and 13 GHz), the generated BBs are clearly deteriorated, and more importantly, the field intensities in the corresponding non-diffraction ranges are significantly weakened, consistent with the efficiency spectra shown in Fig. 2. Figures 3(b)–3(e) depict the corresponding FDTD simulation results in different cases, which are in perfect agreement with the measured results. To check the quality of the generated BB, we also experimentally map out the

transverse field distributions of the beam (at 12 GHz) at different longitudinal positions. Comparisons between our measured patterns and that of an ideal BB demonstrate the good quality of the generated BB (supplementary material).

We now experimentally demonstrate the self-healing property of the generated BB, that is, its propagation behaviors are not affected by small obstacles. Placing a metallic sphere (with diameter $D = 15$ mm) at 55 mm away from the BB generator, we illuminate the metasurface with a left CP wave at 11.8 GHz and then repeat the near-field scanning measurements. Clearly, while the presence of the metallic sphere does scatter the BB in the vicinity of the sphere [Fig. 4(b)], some waves can bypass the scatterer and reconstruct the desired BB field pattern in the far-field. The resulting far-field pattern is nearly identical with that of the original BB [Fig. 4(a)], unambiguously demonstrating the self-healing property. We find that this self-healing effect is quite insensitive to the position of the metallic scatterer, as shown in Fig. 4(c), where the scatterer is shifted to 125 mm from the BB generator. Numerical simulations are in good agreement with the experimental results and further demonstrate that the self-healing effect is insensitive to the shape of the scatterer (supplementary material).

We finally perform far-field experiments to quantify the working efficiency of our device. However, for a device generating a 3D BB, it is difficult to experimentally integrate all the radiation powers within the solid-angle range. Therefore, we fabricate a 2D BB generator based on the same PB meta-atom and deflection angle [Fig. 5(a)] and experimentally determine its working efficiency. In our measurement, we illuminate the sample with a left CP horn antenna and use another CP horn antenna as a receiver to measure the scattered-field distributions. Figures 5(c) and 5(d) depict the far-field power distributions measured with the receiver possessing an opposite and an identical circular polarization to the source, respectively. All experimental data are normalized against a co-polarized signal

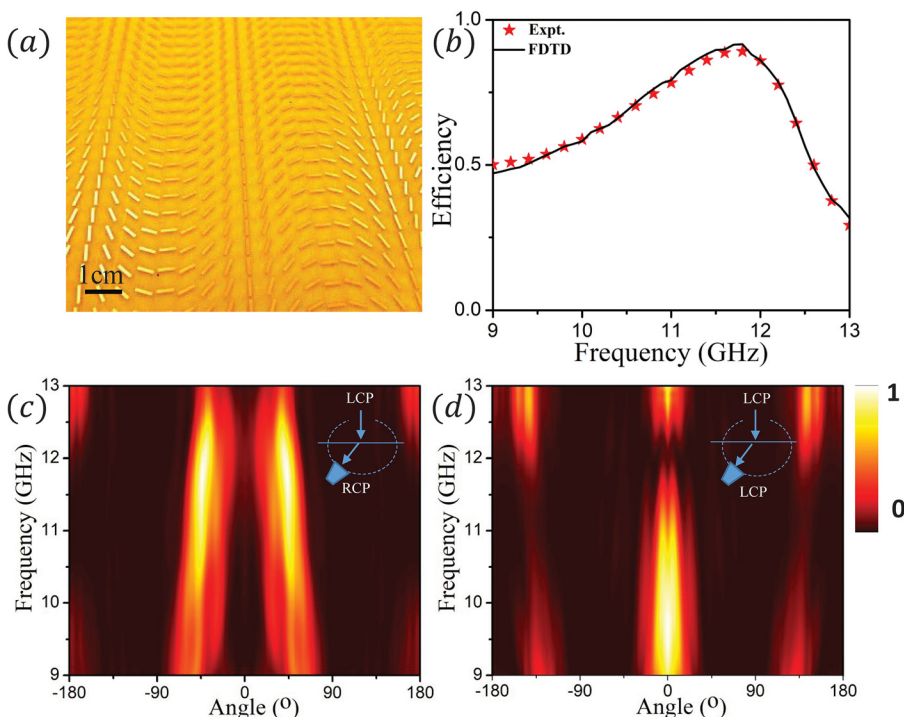


FIG. 5. (a) Photograph of part of the fabricated 2D BB generator. Scattered-field intensity as a function of the detection angle and frequency for the metasurface illuminated by a left CP wave, measured with a right CP receiver (c) or a left CP receiver (d). The angular range of $(-90^\circ, 90^\circ)$ corresponds to the transmission side, with the other range related to the reflection side. (b) Working efficiencies of the PB metasurface calculated from the experimental data shown in (c) and (d).

measured with the sample replaced by an air aperture of the same size. Clearly, the anomalous-transmission modes dominate within the working band (10.7–12.3 GHz), where the signals carried by the other three modes (i.e., the normal-transmission mode and the normal/anomalous-reflection modes) are very weak ([supplementary material](#)). Outside the working band, however, the other modes become significant, degrading the performance of our device. We can determine the working efficiency of this device by integrating the power carried by the anomalous-transmission waves and then dividing it by the total emitted power. Figure 5(d) shows the working efficiency of this device calculated from the experimental data. The efficiency reaches 91% at 12 GHz, agreeing well with FDTD simulations ($\sim 92\%$, [supplementary material](#)) and with the predicted values in Figs. 2(e) and 2(f) based on the meta-atom properties.

In summary, we designed and fabricated ultra-thin metasurfaces and demonstrated both experimentally and by numerical simulations that they can generate non-diffraction and self-healing CP BBs with very high efficiencies within a broad frequency band. Compared with previous schemes generating BBs,^{7–9,21,28} our device is flat and much thinner, exhibits higher working efficiency, and can generate high-quality spin-polarized BBs. Our results may stimulate future work on CP-BB-related applications, such as chiral-particle trapping and manipulation^{5,6} and even optical pulling force³³ generation.

See [supplementary material](#) for FDTD simulations on the self-healing effect of BB generated by our metasurfaces, simulated scattered-field distributions of the 2D BB generator, verifications on the fidelity of the generated BBs, and measured efficiency spectra of our BB generator.

This work was supported by the National Natural Science Foundation of China (Nos. 11474057, 11404063, 11734007, and 11674068), the National Basic Research Program of China (Nos. 2017YFA0303500 and 2017YFA070008), and the Shanghai Science and Technology Committee (Nos. 16ZR1445200, 16JC1403100, and 18ZR1403400).

¹Q. Zhan, *Adv. Opt. Photonics* **1**, 1 (2009).

²F. O. Fahrbach, P. Simon, and A. Rohrbach, *Nat. Photonics* **4**, 780 (2010).

³A. Novitsky, C. W. Qiu, and H. Wang, *Phys. Rev. Lett.* **107**, 203601 (2011).

⁴M. Duocastella and C. B. Arnold, *Laser Photonics Rev.* **6**, 607 (2012).

⁵S. B. Wang and C. T. Chan, *Nat. Commun.* **5**, 3307 (2014).

⁶O. Brzobohatý, A. V. Arzola, M. Šiler, L. Chvátal, P. Jákł, S. Simpson, and P. Zemaněk, *Opt. Express* **23**, 7273 (2015).

⁷D. DeBeer, S. R. Hartmann, and R. Friedberg, *Phys. Rev. Lett.* **59**, 2611 (1987).

⁸S. Monk, J. Arlt, D. A. Robertson, J. Courtial, and M. J. Padgett, *Opt. Commun.* **170**, 213 (1999).

⁹J. Turunen, A. Vasara, and A. T. Friberg, *Appl. Opt.* **27**, 3959 (1988).

¹⁰N. Yu, P. Genevet, M. A. Kats, F. Aieta, J. P. Tetienne, F. Capasso, and Z. Gaburro, *Science* **334**, 333 (2011).

¹¹X. Ni, N. K. Emani, A. V. Kildishev, A. Boltasseva, and V. M. Shalaev, *Science* **335**, 427 (2012).

¹²S. Sun, K. Y. Yang, C. M. Wang, T. K. Juan, W. T. Chen, C. Y. Liao, Q. He, S. Xiao, W. T. Kung, G. Y. Guo *et al.*, *Nano Lett.* **12**, 6223 (2012).

¹³S. Sun, Q. He, S. Xiao, Q. Xu, X. Li, and L. Zhou, *Nat. Mater.* **11**, 426 (2012).

¹⁴G. Zheng, H. Mühlenbernd, M. Kenney, G. Li, T. Zentgraf, and S. Zhang, *Nat. Nanotechnol.* **10**, 308 (2015).

¹⁵W. T. Chen, K. Yang, C. Wang, Y. Huang, G. Sun, C. Y. Liao, W. Hsu, H. T. Lin, S. Sun, L. Zhou *et al.*, *Nano Lett.* **14**, 225 (2014).

¹⁶F. Aieta, M. Kats, A. P. Genevet, and F. Capasso, *Science* **347**, 1342 (2015).

¹⁷X. Chen, L. Huang, H. Mühlenbernd, G. Li, B. Bai, Q. Tan, G. Jin, C. W. Qiu, S. Zhang, and T. Zentgraf, *Nat. Commun.* **3**, 1198 (2012).

¹⁸M. D. Huntington, L. J. Lauhon, and T. W. Odom, *Nano Lett.* **14**, 7195 (2014).

¹⁹X. Ding, F. Monticone, K. Zhang, L. Zhang, D. Gao, S. Nawaz Burokur, A. De Lustrac, Q. Wu, C. W. Qiu, and A. Alù, *Adv. Mater.* **27**, 1195 (2015).

²⁰X. Wan, X. Shen, Y. Luo, and T. J. Cui, *Laser Photonics Rev.* **8**, 757 (2014).

²¹C. Pfeiffer and A. Grbic, *Phys. Rev. Lett.* **110**, 197401 (2013).

²²D. Lin, P. Fan, E. Hasman, and M. L. Brongersma, *Science* **345**, 298 (2014).

²³W. T. Chen, M. Khorasaninejad, A. Y. Zhu, J. Oh, R. C. Devlin, A. Zaidi, and F. Capasso, *Light: Sci. Appl.* **6**, e16259 (2017).

²⁴S. Y. Lee, K. Kim, S. J. Kim, H. Park, K. Y. Kim, and B. Lee, *Optica* **2**, 6 (2015).

²⁵N. Shitrit, I. Bretner, Y. Gorodetski, V. Kleiner, and E. Hasman, *Nano Lett.* **11**, 2038 (2011).

²⁶Z. Liu, Z. Li, Z. Liu, J. Li, H. Cheng, P. Yu, W. Liu, C. Tang, C. Gu, J. Li *et al.*, *Adv. Funct. Mater.* **25**, 5428 (2015).

²⁷W. Luo, S. Xiao, Q. He, S. Sun, and L. Zhou, *Adv. Opt. Mater.* **3**, 1102 (2015).

²⁸X. Li, M. Pu, Z. Zhao, X. Ma, J. Jin, Y. Wang, P. Gao, and X. Luo, *Sci. Rep.* **6**, 20524 (2016).

²⁹L. Huang, X. Chen, H. Mühlenbernd, H. Zhang, S. Chen, B. Bai, Q. Tan, G. Jin, K. W. Cheah, C. W. Qiu *et al.*, *Nat. Commun.* **4**, 2808 (2013).

³⁰S. Xiao, F. Zhong, H. Liu, S. Zhu, and J. Li, *Nat. Commun.* **6**, 8360 (2015).

³¹P. Genevet and F. Capasso, *Rep. Prog. Phys.* **78**, 024401 (2015).

³²W. Luo, S. Sun, H. X. Xu, Q. He, and L. Zhou, *Phys. Rev. Appl.* **7**, 044033 (2017).

³³K. Ding, J. Ng, L. Zhou, and C. T. Chan, *Phys. Rev. A* **89**, 063825 (2014).